Role of indirect-ionization processes in the electron-impact ionization of Fe^{15+}

S. S. Tayal and Ronald J. W. Henry
Department of Physics and Astronomy, Louisiana State University, Baton Rouge, Louisiana 70803-4001
(Received 8 August 1988)

We have investigated the contributions of excitation-autoionization and resonant-excitation-double-autoionization indirect-ionization processes to the electron-impact ionization of Fe^{15+} using a close-coupling approximation. The total ionization cross sections are obtained by adding the cross sections for these indirect processes to the direct-ionization cross sections. Eleven autoionizing levels arising from the $2p^5 3s^2$, $2p^5 3s 3p$, $2p^5 3p^2$, and $2p^5 3s 3d$ configurations, together with the ground $2p^6 3s$ state, are included in the close-coupling expansion. Large numbers of bound terms of appropriate symmetry are included in the expansion to account for the resonant-excitation-double-autoionization process. The present results are in good agreement with the recent crossed-beam measurement.

I. INTRODUCTION

Several theoretical and experimental investigations[1] have emphasized the importance of indirect-ionization processes to the electron-impact ionization of positive ions. It has been shown that the importance of indirect-ionization processes over direct ionization increases substantially with increasing ionic charge along the isoelectronic sequence. Excitation-autoionization and resonant-excitation-double-autoionization (REDA) processes are the important indirect physical mechanisms for ionization which received considerable theoretical and experimental attention in recent years. In the excitation-autoionization process an inner-shell electron is excited to a level above the ionization threshold which can subsequently decay by autoionization, whereas REDA occurs when the incident electron is captured temporarily with simultaneous excitation of an inner-shell electron followed by double autoionization. The inner-shell excitation can cause significant rise in the ionization cross section close to the threshold for the excitation process. The REDA process was first described by LaGattuta and Hahn[2] in connection with the electron-impact ionization of Na-like Fe^{15+} and it gives rise to resonances in the threshold region. The total ionization cross section can be assumed as the sum of direct- and indirect-ionization processes, if the interference between these processes is ignored. Accurate knowledge of electron-impact ionization cross sections is necessary for an understanding of ionization equilibrium or ion abundance, etc., in astrophysical and laboratory plasmas. Apart from any practical applications, the study of indirect-ionization mechanisms is of interest in its own right.

Na-like ions provide interesting and simple cases for the experimental and theoretical study of indirect-ionization processes. Contributions of the indirect processes to the total ionization cross sections of Na-like ions have been considered theoretically by Bely[3] and Moores and Nussbaumer[4] in the Coulomb-Born approximation, while Cowan and Mann,[5] Griffin and co-workers,[6,7] and LaGattuta and Hahn[2] used distorted-wave approximations. Henry and Msezane[8] performed close-coupling (CC) calculations for Mg^+, Al^{2+}, and Si^{3+} ions of the sodium isoelectronic sequence. On the experimental side, Crandall *et al.*[9] measured absolute total ionization cross sections for Mg^+, Al^{2+}, and Si^{3+} ions. They noted significant enhancements in the cross sections near threshold due to the excitation-autoionization process. Recently, Gregory *et al.*[10] reported measured absolute cross sections for electron-impact ionization of Fe^{15+}. They found that the contribution of excitation autoionization to the total ionization cross section is approximately four times the direct-ionization cross sections. However, the results of their measurements do not appear to provide any clear evidence to support the predicted large contribution of the REDA process near the excitation threshold. LaGattuta and Hahn[2] predicted an overall 30–40% contribution of the REDA process to the total ionization. They predicted a larger contribution due to the REDA process over excitation-autoionization and direct-ionization processes in the energy range 750–780 eV. For highly charged ions, the radiative decay rate may compete with the autoionization rate for some transitions and thereby reduces the contributions of indirect-ionization processes.

In view of the existing discrepancy between the theoretical predictions of LaGattuta and Hahn[2] and the most recent crossed-beam measurements of Gregory *et al.*[10] for the contribution of the REDA process to the electron-impact ionization of Na-like Fe^{15+}, and because of the importance of the ionization cross sections in the modeling of the fusion plasmas where these ions are likely to be present as impurity, we carried out a detailed study of both of the indirect-ionization mechanisms in Fe^{15+} using a close-coupling approximation over a wide energy range of 720–1000 eV. We include the most important autoionizing states in the CC expansion. We consider excitation-autoionization reactions of the type where a $2p$ electron is first excited into a $3s$, $3p$, or $3d$ orbital,

$$e^- + Fe^{15+}(1s^2 2s^2 2p^6 3s) \rightarrow Fe^{15+*}(1s^2 2s^2 2p^5 3snl) + e^- , \quad (1)$$

followed by the autoionization

$$Fe^{15+*}(1s^22s^22p^53snl)\rightarrow Fe^{16+}(1s^22s^22p^6)+e^- , \quad (2)$$

and the REDA ionizing process of the type where the incident electron is captured into a resonant state,

$$e^-+Fe^{15+}(1s^22s^22p^63s)\rightarrow Fe^{14+*}(1s^22s^22p^53snln'l') , \quad (3)$$

followed by the sequential double autoionization

$$Fe^{14+*}(1s^22s^22p^53snln'l')\rightarrow Fe^{15+*}(1s^22s^22p^53snl)+e^- , \quad (4)$$

$$Fe^{15+*}(1s^22s^22p^53snl)\rightarrow Fe^{16+}(1s^22s^22p^6)+e^- . \quad (5)$$

In order to consider the REDA process in our calculation we included a large number of bound terms in the CC expansion. We have also taken into account the radiative decay of the autoionization states to the bound state of the Fe^{15+} ion through branching ratios.

II. TARGET WAVE FUNCTIONS

A large number of autoionizing states may contribute to the excitation-autoionization cross sections. We have adopted an *LS* coupling scheme. The autoionizing states arising from the configurations $2p^53s^2$, $2p^53s3p$, $2p^53p^2$, and $2p^53s3d$ are considered in the present close-coupling calculation. These configurations give rise to a total of 29 *LS* states, but 16 of these states would not autoionize in the *LS* coupling. However, it should be noted that the quartet autoionizing states may contribute to the REDA process through the Rydberg series of resonances converging to these states. The $2p^53p^2(^1D)^2F^\circ$ and $2p^53p^2(^1S)^2P^\circ$ states are found to be weakly coupled to other states in our test calculations. We included 11 autoionizing states together with the ground $2p^63s\ ^2S$ state in the CC expansion in our final calculation. We believe that these autoionizing states would give the most important contributions to the indirect processes in the energy region of interest in the present work. We used six orthogonal one-electron orbitals: 1*s*, 2*s*, 2*p*, 3*s*, 3*p*, and 3*d*. The 1*s*, 2*s*, 2*p*, and 3*s* radial functions are those of the $2p^63s\ ^2S$ ground state given by Clementi and Roetti.[11] The 3*p* and 3*d* functions are optimized on the combina-

TABLE I. Parameters for the bound orbitals used in the calculation. Each orbital is a sum of Slater-type orbitals.

Orbital	Coefficient	Power of *r*	Exponent
3*p*	194.627 47	2	9.768 12
	11.776 53	2	14.179 90
	54.076 45	2	23.528 70
	6.522 33	3	4.163 18
	−212.501 54	3	5.510 09
3*d*	186.036 49	3	6.585 71
	26.911 85	3	4.850 41
	−0.791 83	3	4.734 96
	13.687 53	3	4.898 91
	4.775 46	3	4.801 90

TABLE II. Configurations used for each state in the present calculation. The numbers below the configurations give their weights.

State	Configuration, Weight									
^2S	$2p^63s$	$2p^53s(^1P^\circ)3p$	$2p^53s(^3P^\circ)3p$	$2p^53p(^1D)3d$	$2p^53p(^3D)3d$					
$2p^63s\ ^2S$	0.999 88	0.000 83	−0.000 56	0.004 89	0.014 61					
$2p^53s(^1P^\circ)3p\ ^2S$	−0.000 85	0.953 18	−0.272 65	0.121 92	−0.047 35					
$2p^53s(^3P^\circ)3p\ ^2S$	−0.001 85	0.280 21	0.947 88	−0.012 27	0.151 14					
$^2P^\circ$	$2p^53s^2$	$2p^53s(^1P^\circ)3d$	$2p^53s(^3P^\circ)3d$	$2p^53p^2(^3P)$	$2p^53p^2(^1D)$	$2p^53p^2(^1S)$	$2p^53d^2(^1S)$	$2p^53d^2(^1D)$	$2p^53d^2(^3P)$	
$2p^53s^2\ ^2P^\circ$	−0.983 85	0.000 83	0.031 32	−0.009 29	0.006 77	0.174 10	0.024 76	0.000 80	−0.000 06	
$2p^53s(^1P^\circ)3d\ ^2P^\circ$	0.031 24	0.712 18	0.178 95	0.478 72	0.452 67	0.152 26	−0.022 17	−0.044 48	−0.007 49	
$2p^53s(^3P^\circ)3d\ ^2P^\circ$	0.025 71	0.159 50	0.883 45	−0.195 67	−0.382 63	−0.009 91	−0.003 06	0.089 95	0.022 91	
$2p^53p^2(^3P)^2P^\circ$	0.099 09	−0.555 90	0.227 11	0.543 00	0.009 38	0.565 51	−0.107 17	0.020 38	−0.054 18	
$2p^53p^2(^1D)^2P^\circ$	−0.040 11	0.241 91	−0.265 96	0.511 96	−0.766 77	0.126 62	0.025 10	0.040 58	−0.028 03	
^2D	$2p^53s(^1P^\circ)3p$	$2p^53s(^3P^\circ)3p$	$2p^53p(^1S)3d$	$2p^53p(^3S)3d$	$2p^53p(^1P)3d$	$2p^53p(^3P)3d$	$2p^53p(^1D)3d$	$2p^53p(^3D)3d$		
$2p^53s(^1P^\circ)3p\ ^2D$	0.852 63	0.517 32	0.028 86	0.027 92	−0.021 22	−0.007 50	0.045 18	0.035 35		
$2p^53s(^3P^\circ)3p\ ^2D$	0.511 12	−0.841 17	0.034 93	−0.064 45	−0.059 03	0.117 14	0.054 16	−0.075 30		
$^2F^\circ$	$2p^53s(^1P^\circ)3d$	$2p^53s(^3P^\circ)3d$	$2p^53p^2(^1D)$	$2p^53d^2(^1D)$	$2p^53d^2(^3F)$	$2p^53d^2(^1G)$				
$2p^53s(^1P^\circ)3d\ ^2F^\circ$	0.860 80	0.508 20	−0.006 31	0.004 79	0.021 57	0.015 26				
$2p^53s(^3P^\circ)3d\ ^2F^\circ$	0.452 81	−0.761 33	0.450 58	−0.10850	0.007 27	0.022 17				

TABLE III. Excitation energies (eV) of the autoionizing states relative to the ground $2p^6 3s\ ^2S$ state.

State	Energy (eV)
$2p^5 3s^2\ ^2P^\circ$	721.14
$2p^5 3s(^1P^\circ)3p\ ^2D$	750.05
$2p^5 3s(^1P^\circ)3p\ ^2S$	753.48
$2p^5 3s(^3P^\circ)3p\ ^2D$	761.11
$2p^5 3s(^3P^\circ)3p\ ^2S$	774.75
$2p^5 3p^2(^1D)^2P^\circ$	780.42
$2p^5 3p^2(^3P)^2P^\circ$	800.27
$2p^5 3s(^1P^\circ)3d\ ^2P^\circ$	800.38
$2p^5 3s(^1P^\circ)3d\ ^2F^\circ$	807.65
$2p^5 3s(^3P^\circ)3d\ ^2F^\circ$	808.77
$2p^5 3s(^3P^\circ)3d\ ^2P^\circ$	816.31

tion of

$$2p^5 3s(^1P^\circ)3p\ ^2S + 2p^5 3s(^3P^\circ)3p\ ^2S$$

and

$$2p^5 3s(^1P^\circ)3d\ ^2P^\circ + 2p^5 3s(^3P^\circ)3d\ ^2P^\circ$$

states, respectively. Each of these orbitals was expanded in Slater-type orbitals of the form[12]

$$P_{nl}(r) = \sum_i c_i r^{p_i} \exp(-\xi_i r) \ . \tag{6}$$

In Table I we give the parameters of the Slater-type orbitals for the $3p$ and $3d$ functions. In Table II a list of configurations used for each state is given. The coefficient of each configuration in the configuration-interaction (CI) expansion is given below the configuration. It is easily seen from this table that CI effects are very important for the autoionization states, while the mixing in the ground state is very small.

The calculated excitation energies in eV relative to the ground state are presented in Table III. The oscillator strengths for the resonance transitions are given in Table IV. The good agreement between the length and velocity forms of these oscillator strengths provides confidence in the accuracy of wave functions used in the present calculation.

III. COLLISION CALCULATION

The total wave function representing the electron-ion collision is expanded in terms of the N-electron target wave functions X_i and $(N+1)$-electron bound-state configurations ϕ_j by the CC expansion

TABLE IV. Oscillator strengths for allowed transitions.

Transition	Present Calculation f_L	f_V
$^2S \rightarrow 2p^5 3s^2\ ^2P^\circ$	0.087	0.084
$^2S \rightarrow 2p^5 3s(^1P^\circ)3d\ ^2P^\circ$	0.780	0.724
$^2S \rightarrow 2p^5 3s(^3P^\circ)3d\ ^2P^\circ$	2.076	1.980
$^2S \rightarrow 2p^5 3p^2(^1D)^2P^\circ$	0.023	0.026
$^2S \rightarrow 2p^5 3p^2(^1S)^2P^\circ$	0.029	0.032
$^2S \rightarrow 2p^5 3d^2(^1S)^2P^\circ$	0.014	0.015

$$\psi = A \sum_i X_i \theta_i + \sum_j c_j \phi_j \ , \tag{7}$$

where A is the antisymmetrization operator and θ_i are the numerical basis functions describing the motion of the scattered electron. The bound configurations in the second summation are included to account for the REDA process. Application of a variational principle leads to a set of coupled integrodifferential equations which are solved numerically by the R-matrix method.[13,14] In the R-matrix method the configuration space is partitioned into two regions. In the inner region electron exchange and correlation effects are taken into account, while in the outer region electron exchange effects are ignored. A zero logarithmic derivative was imposed at the boundary $a = 2.6$ a.u. on the continuum basis functions. Twenty-two continuum orbitals of each angular symmetry were included, giving good convergence in the energy range of interest. Each term in the first summation of Eq. (7) gives rise to an interaction channel. The largest number of channels included is 27 in the present work. The bound configurations in the second summation of Eq. (7) were obtained by adding the scattering electron in all possible ways to the configurations included in the description of target states, consistent with the total orbital angular momentum (L), spin (S), and parity (Π).

Assuming the direct- and indirect-ionization processes to be independent we can calculate the total ionization cross section by the relation

$$\sigma_{\text{tot}} = \sigma_{\text{direct}} + \sum_j \sigma^j_{\text{excit}} B^a_j \ , \tag{8}$$

where σ_{direct} is the direct ionization cross section, σ^j_{excit} is the excitation cross section to the j autoionizing state, and B^a_j is the branching ratio for autoionization from the level j. We are interested in the excitation cross sections for the transitions of the type

$$^2S \rightarrow 2p^5 3s^2\ ^2P^\circ, \ 2p^5 3s(^{1,3}P^\circ)3p\ ^2D, ^2S, \ 2p^5 3p^2(^3P, ^1D)^2P^\circ, \ 2p^5 3s(^{1,3}P^\circ)3d\ ^2P^\circ, ^2F^\circ \ .$$

The branching ratio is given by

$$B^a_j = \frac{\sum_m A_a(j \rightarrow m)}{\sum_m A_a(j \rightarrow m) + \sum_k A_r(j \rightarrow k)} \ , \tag{9}$$

where $A_a(j \rightarrow m)$ is the autoionization rate from level j to the continuum channel m, and $A_r(j \rightarrow k)$ is the radiative rate from level j to a bound state k. As we mentioned in the Introduction, for highly charged Fe^{15+} the radiative rate may not be negligible and this would result in a nonunity value of the branching ratios. Griffin has provided us the branching ratios which he calculated us-

ing the configurations and eigenvector components given in Table II. Griffin *et al.*[7] found that the branching ratios are very sensitive to the CI and intermediate coupling effects. We included one-electron Darwin and mass-correction relativistic terms in the present semirelativistic calculation in the Breit-Pauli approximation. The inclusion of spin-orbit interaction will give rise to a large number of channels. The spin-orbit interaction, therefore, is not included to keep the calculation manageable. A fully relativistic calculation in the framework of the close-coupling approximation would need a tremendous amount of computer time and memory.

IV. RESULTS AND DISCUSSION

An estimate of the direct-ionization cross sections in Fe^{15+} can be obtained by the use of the Lotz formula.[15] However, we have used more reliable distorted-wave cross sections for the direct ionization of valence $3s$ electron in our calculation. These were obtained by using Younger's formula[16] and the parameters given by Pindzola *et al.*[17] The distorted-wave results for direct ionization are about 15% lower than the prediction of the Lotz formula. The inner-shell excitation cross sections for the $2p \rightarrow 3s$, $2p \rightarrow 3p$, and $2p \rightarrow 3d$ transitions are given in Table V for energies from 816.5 to 952.0 eV. It is clear from this table that $2p \rightarrow 3d$ transitions give the dominant contribution to the excitation autoionization. In this table we have also listed the ratios of indirect to direct cross sections which are in excellent agreement with the experimental estimates of Gregory *et al.*[10]

The results of our calculation for the electron-impact ionization of Fe^{15+} are displayed in Fig. 1, where they are compared with the experimental data of Gregory *et al.*[10] The dashed curve gives the distorted-wave direct-ionization cross sections. The solid and dotted curves represent the present results obtained by adding the direct-ionization cross sections to the excitation cross sections with unit and nonunit branching ratios, respectively, in Eq. (8). The radiative decay of the autoionizing levels to the bound levels of Fe^{15+} is found to reduce the excitation cross sections by about 5%. We considered inner-shell excitations of the type $2p^6 3s \rightarrow 2p^5 3snl$ ($n=3$), while Griffin *et al.*[7] considered additional inner-shell excitations of the type $2p^6 3s \rightarrow 2p^5 3snl$ ($n=4,5$) and $2s^2 2p^6 3s \rightarrow 2s 2p^6 3snl$ ($n=3,4$) in their distorted-wave calculations. The $3l$ excited states would make dominant contributions to excitation autoionization. The excitation-autoionization features associated with the $4l$, $5l$, and higher excited states should be smaller than those for the $3l$ excited states and would occur at higher energies. A comparison of the present CC results with the distorted wave results of Griffin *et al.*[7] (not shown) in the energy region from 825 to 935 eV (that is, before the onset of $4l$ excitations) indicates that the present results are 10–15% larger than their results. Their results are lower than the measurement and the present results at energies $E < 800$ eV. It should be noted that Griffin *et al.*[7] did not include the REDA process in their calculation. Our calculation shows resonance structure due to the REDA process in the energy region from 720 to 816 eV. These resonances occur as Rydberg series below each of the excited states included in the present work. We calculated excitation cross section at 698 energy

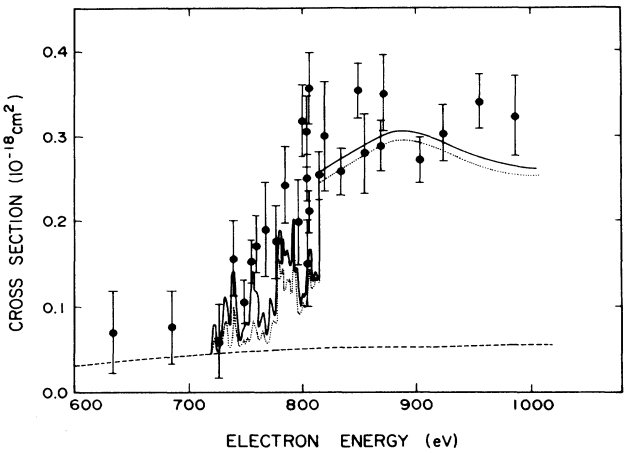

FIG. 1. Electron-impact ionization cross section for the ground $2p^6 3s\ ^2S$ state of Fe^{15+}. Solid curve, present CC cross sections with unit branching ratios; dotted curve, present CC cross sections with nonunit branching ratios; dashed curve, distorted-wave direct-ionization cross sections; solid circles, experimental results (Ref. 10).

TABLE V. Cross sections for the inner-shell excitations $2p^6 3s \rightarrow 2p^5 3s 3l$ ($l=0,1,2$).

Electron energy (eV)	Cross sections (10^{-18}cm^2) transition $2p \rightarrow 3s$	$2p \rightarrow 3p$	$2p \rightarrow 3d$	total	Ratios of indirect to direct cross sections
816.5	0.004	0.047	0.156	0.207	4.1
829.6	0.004	0.049	0.160	0.213	4.2
843.2	0.004	0.053	0.168	0.225	4.3
856.8	0.004	0.055	0.178	0.237	4.5
870.4	0.004	0.057	0.186	0.247	4.7
897.6	0.004	0.053	0.191	0.248	4.6
924.8	0.004	0.049	0.185	0.238	4.4
952.0	0.004	0.048	0.169	0.221	4.0

points using a fine energy mesh (0.01 eV) in this energy region. These cross sections are then convoluted with a 2-eV full width at half maximum Gaussian to simulate experimental energy spread. Our convoluted results appear to be in reasonable agreement with the experiment except at energies around 800 eV where the experiment indicates some large structure. The position of resonances may be shifted in comparison to the measurement because of the difference in theoretical and experimental threshold energies. Our results with branching ratios (dotted curve) may be in error for energies $E < 816$ eV due to the fact that we assumed a unit branching ratio for the autoionization of resonant levels of Fe^{14+*} to the autoionizing levels of Fe^{15+*} [Eq. (4)]. LaGattuta and Hahn predicted much larger REDA contributions to the cross section than the present calculation and the measurement of Gregory *et al.*[10] Mann[18] calculated electron-impact excitation cross sections using a distorted-wave approximation. When his results are added to the direct-ionization cross sections, they are found to overestimate the cross sections. His results are typically 20% larger than the present results at 900 eV.

In conclusion, we have presented electron-impact ionization cross sections for Na-like Fe^{15+} over the energy region from 720 to 1000 eV. We considered both excitation-autoionization and resonant-excitation-double-autoionization indirect-ionization processes in our calculation. The present results are in good agreement with the recent crossed-beam measurement of absolute ionization cross sections. Our calculation does not show large resonance enhancements due to the REDA process, in disagreement with the prediction of LaGattuta and Hahn. It is possible that the inclusion of quartet autoionizing states may decrease this disagreement. This may be the subject of a future, much larger calculation in which all autoionizing states arising from the configurations $2p^5 3s^2$, $2p^5 3s 3p$, and $2p^5 3s 3d$ will be included in the close-coupling expansion. In order to keep the calculation manageable, we were forced to make various simplifying assumptions which may introduce some errors in the present results, the important one being the omission of spin-orbit interaction from the Hamiltonian. We have neglected the interference between direct- and indirect-ionization processes. We have also ignored the post collision interactions between the scattered and ionizing electrons in our work.

ACKNOWLEDGMENTS

We are grateful to D. C. Griffin for providing us the branching ratios compatible with our calculation. This research was supported in part by the U.S. Department of Energy (Division of Chemical Sciences).

[1]For example, see O. Bely, Ann. Astrophys. **30**, 953 (1967); D. H. Crandall, Phys. Scr. **23**, 153 (1981); D. H. Crandall, R. A. Phaneuf, D. C. Gregory, A. M. Howald, D. W. Mueller, T. S. Morgan, G. H. Dunn, and R. J. W. Henry, Phys. Rev. A **34**, 1757 (1986); R. A. Falk, G. H. Dunn, D. C. Griffin, C. Bottcher, D. C. Gregory, D. H. Crandall, and M. S. Pindzola, Phys. Rev. Lett. **47**, 494 (1981); S. S. Tayal and R. J. W. Henry, Phys. Rev. A **33**, 3825 (1986).

[2]K. J. LaGattuta and Y. Hahn, Phys. Rev. A **24**, 2273 (1981).

[3]O. Bely, J. Phys. B **1**, 23 (1968).

[4]D. L. Moores and H. Nussbaumer, J. Phys. B **3**, 161 (1970).

[5]R. D. Cowan and J. B. Mann, Astrophys. J. **232**, 940 (1979).

[6]D. C. Griffin, C. Bottcher, and M. S. Pindzola, Phys. Rev. A **25**, 154 (1982).

[7]D. C. Griffin, M. S. Pindzola, and C. Bottcher, Phys. Rev. A **36**, 3642 (1987).

[8]R. J. W. Henry and A. Z. Msezane, Phys. Rev. A **26**, 2545 (1982).

[9]D. H. Crandall, R. A. Phaneuf, R. A. Falk, D. S. Belic, and G. H. Dunn, Phys. Rev. A **25**, 143 (1982).

[10]D. C. Gregory, L. J. Wang, F. W. Meyer, and K. Rinn, Phys. Rev. A **35**, 3256 (1987).

[11]E. Clementi and C. Roetti, At. Data Nucl. Data Tables **14**, 177 (1974).

[12]A. Hibbert, Comput. Phys. Commun. **9**, 141 (1975).

[13]P. G. Burke, A. Hibbert, and W. D. Robb, J. Phys. B **4**, 153 (1971).

[14]K. A. Berrington, P. G. Burke, M. LeDourneuf, W. D. Robb, K. T. Taylor, and Vo Ky Lan, Comput. Phys. Commun. **14**, 367 (1978).

[15]W. Lotz, Z. Phys. **216**, 241 (1968).

[16]S. M. Younger, Phys. Rev. A **24**, 1272 (1981).

[17]M. S. Pindzola, D. C. Griffin, C. Bottcher, S. M. Younger, and H. T. Hunter, Oak Ridge National Laboratory Report No. ORNL/TM-10297, 1987 (unpublished).

[18]J. B. Mann, At. Data Nucl. Data Tables **29**, 407 (1983).